ChemBioChem

Research Article
doi.org/10.1002/cbic.202300320

Chemistry Europe
European Chemical Societies Publishing

www.chembiochem.org

A RaPID Macrocyclic Peptide That Inhibits the Formation of α-Synuclein Amyloid Fibrils

Tatsuya Ikenoue,*[a] Miki Oono,[b] Masatomo So,[c] Hodaka Yamakado,[b] Toshiaki Arata,[c, d] Ryosuke Takahashi,[b] Yasushi Kawata,[e] and Hiroaki Suga*[a]

There is considerable interest in drug discovery targeting the aggregation of α-synuclein (αSyn) since this molecular process is closely associated with Parkinson's disease. However, inhibiting αSyn aggregation remains a major challenge because of its highly dynamic nature which makes it difficult to form a stable binding complex with a drug molecule. Here, by exploiting Random non-standard Peptides Integrated Discovery (RaPID) system, we identified a macrocyclic peptide, BD1, that could interact with immobilized αSyn and inhibit the formation of fibrils. Furthermore, improving the solubility of BD1 suppresses the co-aggregation with αSyn fibrils while it kinetically inhibits more effectively without change in their morphology. We also revealed the molecular mechanism of kinetic inhibition, where peptides bind to fibril ends of αSyn, thereby preventing further growth of fibrils. These results suggest that our approach for generating non-standard macrocyclic peptides is a promising approach for developing potential therapeutics against neurodegeneration.

Introduction

Alpha-synuclein (αSyn) is an intrinsically disordered protein that self-assembles into amyloid fibrils, which are the major components of the Lewy body representing a molecular hallmark of Parkinson's disease.[1] Although inhibiting the aggregation of αSyn and their associated toxicity has been explored as a major therapeutic strategy against Parkinson's disease,[2] effective or promising molecules that prevent the disease via such an inhibitory action have not yet become available.

It is challenging to develop effective strategies to modulate the formation of amyloid fibrils,[2a,3] because the mechanism of protein aggregation is complex. A series of efforts to clarify the mechanism for the formation of amyloid fibrils revealed that there is a long lag time in spontaneous fibril formation and rapid fibril formation by the addition of preformed fibrils, suggesting a similarity with the supersaturation-limited crystallization of substances.[4] In the case of αSyn, this process involves the following three states, a highly disordered monomeric state, a transient and cytotoxic oligomeric state, and an ordered stable fibril state.[5]

For the inhibition of amyloid-β (Aβ) aggregation, which is one of the hallmarks of Alzheimer's disease, targeting the fibril states is suggested as a strategy that suppresses the formation of oligomeric species catalyzed by fibril surface.[6] Some designed peptides have been shown that can cap fibrils to prevent the addition of further monomeric units, which antagonize the aggregation and reduce amyloid toxicity.[7] On the other hand, targeting monomeric state of disordered proteins, such as αSyn, is still challenging although it may affect the initial step of aggregation and suppress the subsequent formation of toxic species.[8] Monomeric form of αSyn is intrinsically disordered and lacks permanent structure, thus they do not readily lead to a conventional enthalpy-focused mechanism of binding, as shown for Aβ.[9] The fibril state of αSyn may also have difficulty in targeting because highly charged N-terminus (1–37) and C-terminus (98–140) are not well-defined by structural studies of fibril using NMR and cryo-EM,[10] suggesting that a dense mesh of disordered tails surround the structured core of fibril. These features have made it difficult to achieve screening to obtain *de novo* binders because they have to overcome large entropic loss upon the binding.

Several peptides, such as engineered polypeptides inspired by native amyloidogenic sequences, have been designed to prevent growth of the fibrils. However, to our knowledge, an αSyn-specific *de novo* peptide inhibitor, developed by experimental approaches, has not yet been reported. Various discovery strategies are currently available for the discovery of cyclic peptides against given targets. The random non-standard

[a] *Dr. T. Ikenoue, Prof. H. Suga*
Department of Chemistry, The University of Tokyo
Tokyo 113-0033 (Japan)
E-mail: t-ikenoue@chem.s.u-tokyo.ac.jp
hsuga@chem.s.u-tokyo.ac.jp
[b] *Dr. M. Oono, Dr. H. Yamakado, Prof. R. Takahashi*
Department of Neurology, Kyoto University Hospital
Kyoto 606-8507 (Japan)
[c] *Dr. M. So, Prof. T. Arata*
Institute for Protein Research, Osaka University
Osaka 565-0871 (Japan)
[d] *Prof. T. Arata*
Graduate School of Science
Osaka Metropolitan University
Osaka 558-8585 (Japan)
[e] *Prof. Y. Kawata*
Department of Chemistry and Biotechnology
Tottori University
Tottori 680-8552 (Japan)

Supporting information for this article is available on the WWW under https://doi.org/10.1002/cbic.202300320

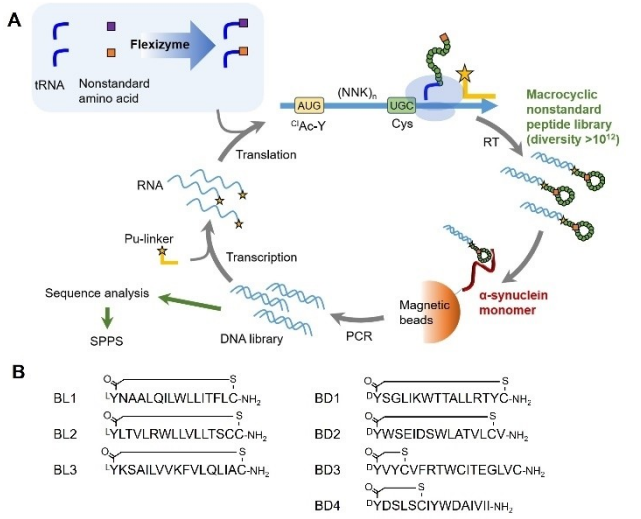

Figure 1. In vitro selection of noncanonical cyclic peptides against αSyn by RaPID system and selected macrocyclic peptides. (*A*) Overview of RaPID system for macrocyclic peptides. Messenger RNA libraries containing a random sequence domain, $(NNK)_{4-9}$ and $(NNK)_{10-15}$, were transcribed from the corresponding cDNA library and conjugated with an oligonucleotide bearing puromycin. The resulting mRNAs were translated by the FIT system in the presence of the appropriate aminoacyl–tRNAs prepared by flexizymes. Linear peptides displayed on the individual mRNAs were spontaneously cyclized after translation, resulting in macrocyclic peptides being displayed. Reverse transcription was performed before selection. The peptide libraries were then subjected to $(His)_6$-αSyn immobilized on magnetic beads, and binding species were isolated. The cDNAs on the binding mRNA–peptide fusion were recovered and amplified by PCR. (*B*) Peptide sequences were identified from the pool in round 10.

peptides integrated discovery (RaPID) system[11] (Figure 1A) uses the combination of messenger RNA display and genetic code reprogramming facilitated by the flexible in vitro translation, referred to as FIT, system.[12] This system enables the ribosomal synthesis of extremely large ($>10^{12}$ compound) libraries of natural product-like macrocyclic peptides and rapid selection based on binding to protein targets of interest. Even though we witnessed a number of successful discoveries of various types of proteins, including enzymes, membrane proteins, secreted proteins, and intracellular proteins involved in protein–protein interaction, we had not yet applied the RaPID system for selecting macrocycles against a highly dynamic protein that self-aggregates. However, since the conformationally restrained structure of such macrocycles would lead to a relatively small entropy cost upon binding and achieve potent binding affinity and high specificity,[13] we envision that this approach may yield adequate macrocycles capable of interfering with the protein–protein interaction occurring in the aggregates, potentially yielding an inhibitor for the fibril formation.[14]

Results and Discussion

RaPID selection of macrocyclic peptides against monomeric α-Syn

We performed the RaPID selection to identify macrocycles based on their ability to interact with αSyn (Figure 1A). A puromycin-ligated mRNA library was constructed to encode macrocyclic peptides with N-chloroacetyl-L-Tyrosine (^{L}Y-library) or N-chloroacetyl-D-Tyrosine (^{D}Y-library) as an initiator followed by a random peptide region consisting of 4–9 residues or 10–15 residues, followed by cysteine and ending with a short linker peptide; and thus, a total of four different libraries were used for this selection campaign. Upon translation of these mRNAs, the chloroacetyl group on the N-terminus of the linear peptides spontaneously cyclizes with their downstream cysteine to form thioether-macrocyclic peptides. The respective macrocyclic peptide was covalently linked to the cognate mRNA template via the puromycin linker for cDNA synthesis followed by PCR amplification. Each library was applied to the protein-free magnetic beads to remove background nonspecific binders, and then to αSyn tagged with His6 at the N-terminal region immobilized on the magnetic beads to enrich specific binders to the monomeric state of αSyn.

We performed the RaPID selection using the aforementioned four libraries, but to our surprise, only ^{D}Y-library consisting of 10–15 random residues yielded a successful enrichment of active species selectively binding to the immobilized αSyn over the background (Figure S1). In other libraries, nonspecific binders to beads were dominated in enrichment. In our many selection cases in the past, we often succeeded in the enrichment of active species from both ^{D}Y- and ^{L}Y-libraries, so this was a rare case. Nevertheless, sequence alignment analysis of the 7–10 rounds of the enrich species in ^{D}Y-library revealed four converged classes of macrocyclic peptides were shown in Figure 1B, and we selected a peptide, BD1, for further experiments based on two reasons; (1) it has the most converged sequence, and (2) the highest 'theoretical' score of water solubility. BD1 was chemically synthesized and its solubility in PBS buffer was verified by means of turbidimetry, far-UV circular dichroism (CD) spectroscopy, and atomic force microscopy (AFM) (Figure S2A–C). The results showed that BD1 does not form any large assemblies under the conditions where αSyn could form characteristic fibrils.

BD1 delays the fibril formation of αSyn and changes the aggregation morphology

The aggregation pathways of disordered proteins have been classified into two types, amyloid fibril formation and non-amyloidogenic aggregation. The kinetics of amyloid formation are typically separated into nucleation and elongation phases. The nucleation phase is the duration which is observed as a lag time and is often long because of its high energy barrier. Once nuclei of fibrils are formed, the elongation of fibrils proceeds quite rapidly. Non-amyloidogenic aggregation, e.g. amorphous

aggregation, is formed without a lag time; therefore, it generally competes with the slow nucleation-dependent amyloid formation, producing kinetic complexity of amyloid formation process.[15] In order to investigate the effect of BD1 on the fibril formation of αSyn, we next carried out standard *in vitro* assays using the fluorescent dye thioflavin T (ThT) as an amyloid-sensitive probe and 8-anilino-1-naphthalenesulfonic acid (ANS) as a probe for amorphous aggregates. The hydrophobic probe ANS can also stain amyloid fibrils. The fibril formation of αSyn at the concentration of 100 μM was monitored in the presence of various molar ratios (from 0.01 to 1 molar equivalent) of BD1 at 37 °C (Figure 2A–C). We then confirmed the formation of fibrils by means of far-UV CD spectrometry and AFM (Figure 2E, and F). BD1 clearly affected both the spontaneous fibril formation of αSyn (Figure 2A) and the growth reaction examined by seeding experiments using 5% seeds of αSyn fibrils (Figure 2D). Moreover, BD1 was able to expand the lag time derived from the half-time of aggregation ($t_{1/2}$) (Figure 2B), implying that it affected the early phase of fibril formation. Furthermore, the apparent growth rate of fibril in the seeding experiment was reduced by an increase in the BD1 concentrations (0.02–1.0 molar equivalents, Figure 2D), indicating that the growth phase of fibrils formation was also inhibited by BD1.

We also compared the intensity of ThT and ANS in the presence of various concentrations of BD1 (Figure 2C) and the individual ThT and ANS fluorescence profiles (Figure S3A). BD1 affected the ThT intensity, but did not affect ThT signal nor interfere with the ThT binding to fibrils (Figure S3B). In the presence of BD1 below 0.2 molar equivalents, the magnitude of the ThT fluorescence decreased as the concentration of BD1 increased, whereas the initial ANS fluorescence increased at 0.5 and 1 molar equivalents of BD1 (Figure 2C). These results suggest that the binding of BD1 to αSyn at a concentration greater than 0.5 molar equivalents possibly induces a morphological change into amorphous aggregates accompanying the characteristic feature of rapid aggregation without lag time.[15] Indeed, far-UV CD spectroscopy (Figure 2E) and AFM (Figure 2F) after each incubation at each concentration of BD1 tested showed a morphological transition from fibrillar to non-fibrillar aggregates at 0.5 and 1.0 molar equivalents of BD1. This disturbance of such fibril structures could be caused by the incorporation of BD1 into the αSyn aggregates.[16] On the other hand, a concentration of BD1 lower than 0.5 molar equivalents kinetically delays the fibril formation.

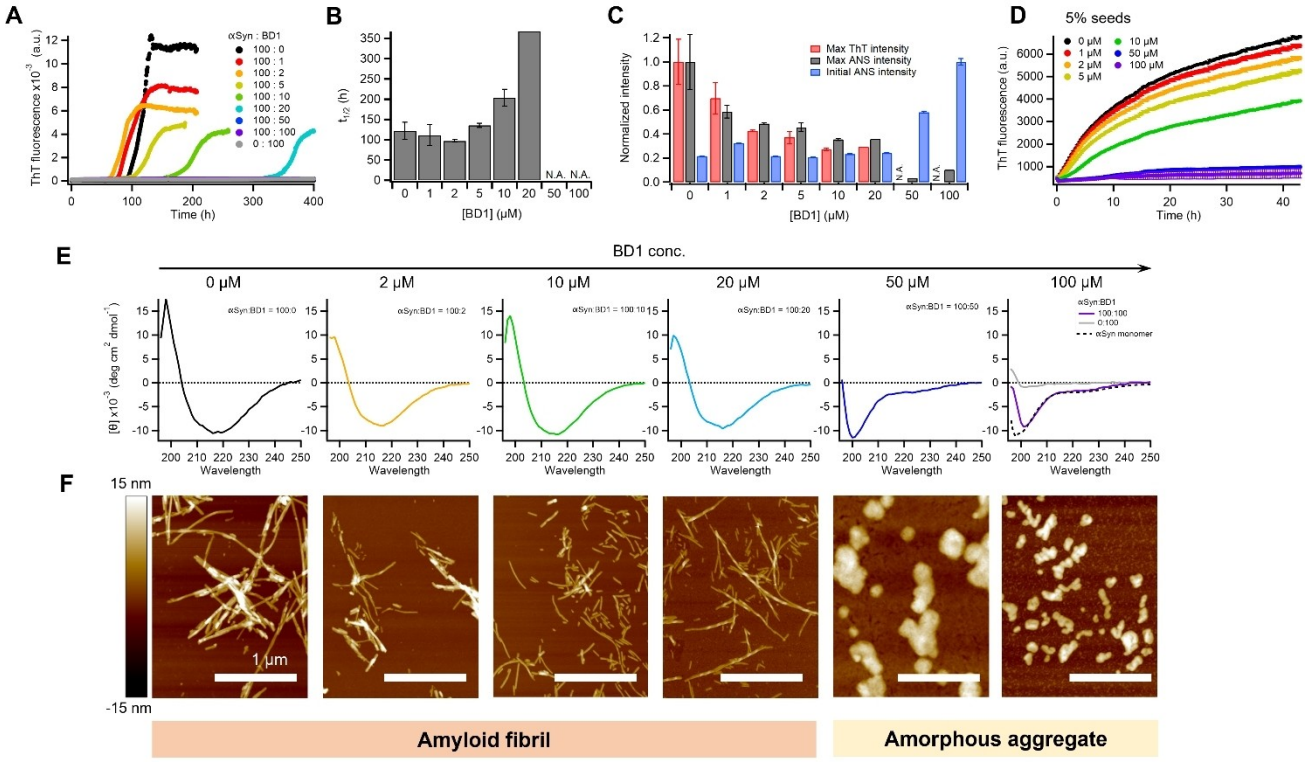

Figure 2. Modulation of the aggregation process of αSyn by BD1. (*A*) ThT kinetic profile of αSyn aggregation with shaking at a concentration of 100 μM in the absence and the presence of various concentrations (1–100 μM) of BD1 (represented by different colors). Representative profiles of three replicants are shown. (*B*) Half-time ($t_{1/2}$) of spontaneous aggregation at each concentration of BD1. The $t_{1/2}$ value at 50 and 100 μM was not available because ThT fluorescence intensity did not show any increment in this time scale. Error bars of arithmetic averages represent STD. (*C*) Normalized maximum ThT (red bar) and ANS (black bar) fluorescence intensity and initial ANS intensity (blue bar) at each BD1 concentration represented in the unseeded aggregation profile. (*D*) Seeded aggregation assay in the presence of 5% αSyn fibrils at a concentration of 50 μM αSyn under quiescent conditions with various concentrations of BD1. (*E*, *F*) Structural feature of αSyn aggregates formed at 100 μM in the presence of various concentrations of BD1. Far-UV CD spectra (*E*) and AFM images (*F*) of αSyn aggregates formed in the absence and presence of various concentrations of BD1. The scale bars on the AFM images indicate 1 μm and scale exhibited at the left represents the height.

Solubility tags attached to BD1 enhance its inhibitory activity for the aggregation of αSyn

In order to avoid co-aggregation of BD1 with αSyn and unify the inhibition mechanism into kinetic inhibition shown at low concentrations of BD1 (Figure 2), we prepared peptides with a solubility tag, BD1–GKKK at the C-terminus (Figure 3A). Because the C-terminus of BD1 was originally attached to a $(GS)_3$-linker followed by mRNA via puromycin (Figure 1A), the modification of this site would not interfere with the binding ability of BD1 to αSyn, expecting that the tag only contributes to the solubility of BD1. Solubility of BD1–GKKK was first evaluated by turbidimetry, demonstrating that their solubility in PBS buffer increased by the tag, particularly at higher concentrations above 100 μM (Figure 3B). We then analyzed the effect of BD1–GKKK on the formation of aggregates/fibrils of αSyn and their morphologies by ThT assay and AFM, respectively (Figure 3C). In the presence of 10–100 μM BD1–GKKK with 100 μM αSyn (0.1–1 : 1 molar ratio of BD1–GKKK:αSyn), the formation of αSyn fibrils was completely inhibited even in the presence of 10 μM. The AFM images taken in the presence of 10, 20, 50, and 100 μM, indeed indicate that no large aggregate is formed under these conditions. These results suggest that the inhibitory effects of BD1 upon αSyn fibril formation would vary depending on the aggregation of BD1 itself.

We also monitored the aggregation of insulin and Aβ40 in the presence of BD1–GKKK, showing nearly no change in aggregations (Figure S4A, B). This indicates that BD1–GKKK is a selective inhibitor of the formation of αSyn fibrils. Moreover, we scrambled the sequence of BD1–GKKK (scrBD1–GKKK) and tested for the inhibition of fibril formation (Figure S4C, D). As expected, scrBD1–GKKK did not show any inhibitory effect for the aggregation, indicating that the specific sequence of BD1 plays a critical role in exhibiting the inhibition.

Characterization of the interaction of BD1–GKKK with monomeric αSyn

We next conducted NMR studies on the interaction between αSyn and BD1–GKKK in order to get a better understanding of the mode of their interaction. We first took ^{1}H-^{15}N HSQC spectra of 100 μM of ^{15}N-labeled αSyn in the presence and absence of 100 μM BD1–GKKK (Figure S5A). These spectra showed nearly no chemical shift perturbation (Δδ) of the respective cross-peaks (Figure S5B), suggesting that the interaction between BD1–GKKK and αSyn is rather weak even though 10 μM of peptide completely inhibits the fibril formation. A similar observation of lacking chemical shift perturbation has been also observed for small compounds known to interact with αSyn.[6b,c,9a,17]

Next, we performed electron spin resonance (ESR) measurements to elucidate the interaction of BD1–GKKK with the fibril state of αSyn. We replaced the G residue of GKKK with cysteine, referred to as BD1–CKKK, in order to attach a nitroxide spin-label, (1-oxyl-2,2,5,5-tetramethylpyrrolidin-3-yl)methyl methanethiosulfonate (MTSL) at the sidechain thiol. The ESR measurements were performed at 25 μM BD1–C*KKK (* denoted *S*-MTSL group on the C's sidechain) in the absence and presence of 100 μM monomeric or fibril state αSyn (Figure 4A). The data showed no change between the spectrum of BD1–C*KKK in the absence and presence of monomeric αSyn, which is consistent with the results of NMR indicating the absence of strong interaction. However, the ESR spectrum in the presence of αSyn fibrils showed the existence of strongly immobilized species, suggesting that BD1–C*KKK bound to αSyn fibrils. We estimated the population of immobile species from the spectrum from which the monomeric spectrum was subtracted to be 93.0% BD1–C*KKK bound to αSyn fibrils.

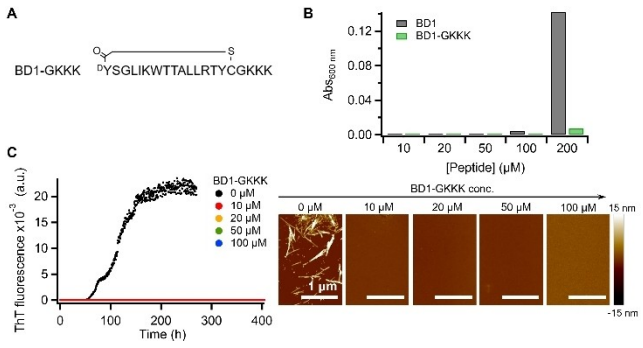

Figure 3. A solubility tagged BD1 peptide that inhibits αSyn fibril formation. (*A*) Amino acid sequences of BD1–GKKK. (*B*) Turbidimetry of BD1 (black) and BD1–GKKK (green) monomers at various concentrations (10–200 μM). (*C*) ThT kinetic profile of formation of αSyn amyloid fibrils at 100 μM in the absence and the presence of various concentrations (10–100 μM) of BD1–KKK. Representative data are shown on each ThT assay from 5 replicates. All profiles in the presence of BD1–GKKK (red, orange, green, and blue) indicated no increase and overlapped with data points of 10 μM (red). Representative AFM images of formed aggregates are shown on the right. The scale bar on the AFM images indicates 1 μm and scale exhibited at the right represents the height.

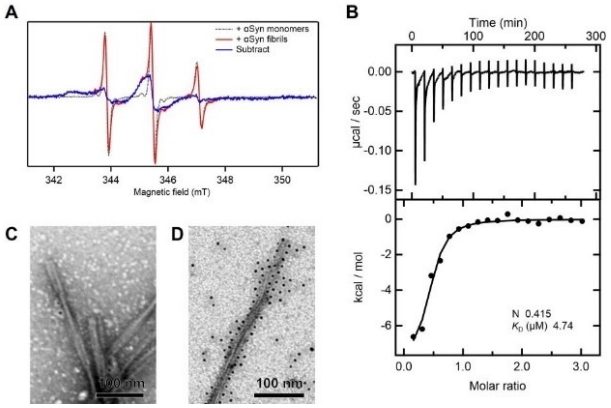

Figure 4. Interaction between BD1–GKKK and fibril state of αSyn. (*A*) ESR spectra of MTSL labeled BD1–C*KKK in the presence of monomeric (black dashed line) and fibril (red solid line) state of αSyn. Subtracted spectrum is shown in a blue solid line. (*B*) ITC thermogram of titration of BD1–GKKK to αSyn amyloid fibrils. (*C, D*) TEM images of amyloid fibrils of αSyn in the absence (*C*) and presence of BD1–GKKKC^{glod} (*D*). Black dots localized around fibrils in *D* show the 5 nm gold nanoparticles which are labeled with each peptide while the sample shown in *C* contains the same concentration of gold nanoparticles without peptides. Scale bars represent 100 nm each.

To estimate the binding affinity of BD1–GKKK to the fibril state of αSyn, we performed isothermal titration calorimetry (ITC) (Figure 4B). A dissociation constant (K_D) was estimated to be 4.7 μM with a small negative binding entropy, which can be obtained by combining with ΔH value calculated from the peak area ($\Delta G_{app} = -RT\ln(1/K_D) = \Delta H - T\Delta S$) (Figure S5C).

To this end, we wanted to confirm the localization of peptides on the surface of αSyn fibrils by means of transmission electron microscopy (TEM). To visualize the position of BD1–GKKK peptide in the TEM images, we added a cysteine residue at the C-terminus BD1–GKKK, BD1–GKKKC, which was labeled with 5 nm of gold nanoparticle (BD1–GKKKC^{glod}). The representative TEM images of fibrils in the presence of the gold nanoparticle alone (Figure 4C) showed no localization of the surface of αSyn fibrils. On the other hand, the BD1–GKKKC^{glod} clearly localized on the surface of αSyn fibrils (Figure 4D). The data suggests that the BD1–GKKK peptide interacts with the surface of αSyn fibrils, resulting in the inhibition of the growth of fibrils.

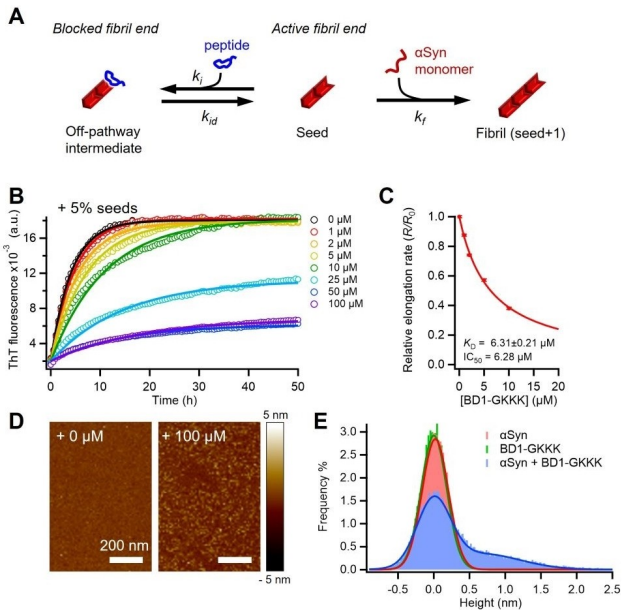

Figure 5. Kinetic analysis of elongation of αSyn fibril inhibited by BD1–GKKK. (*A*) A reaction model representing the interaction of BD1–GKKK and elongation of α-synuclein fibril. (*B*) Kinetic profile of seeded aggregation assay in the presence of 5 %α-synuclein fibrils at a concentration of 50 μM αSyn monomers under quiescent conditions with various concentrations of BD1–GKKK. (*C*) Relative rates of fibril elongation at various concentrations. (*D, E*) AFM images of the initial state of αSyn in the absence and presence of BD1–GKKK (*D*) and histogram of the height of assemblies (*E*). Fitted Gaussian curves are drawn as eye-guide. The curve for the blue histogram is created with the multi-peak fit.

Kinetic analysis of fibril formation of αSyn

To obtain more insight into the microscopic steps of αSyn aggregation affected by BD1–GKKK, we next applied a kinetic analysis to seeding experiments. Since the number of reactive fibril ends should not be influenced by quiescent conditions, we have applied a simplified reaction model which is analogous to competitive inhibition of enzyme catalysis[18] (Figure 5A, see the Supporting Information) where k_i and k_{id} are the rate constants for association and dissociation of BD1–GKK to active fibril end, respectively, while k_f is the rate constants for elongation of the fibril. Here, based on the result of interaction analysis, we assumed off-pathway intermediate is a state that the elongation terminus of fibrils is capped with BD1–GKKK, as shown by αSyn[18a] and other amyloidogenic proteins.[19] If the blocking of fibril end by BD1–GKKK is a fast equilibrium process, the fibril formation rate is determined by the equilibrium concentration of free fibril ends (Supporting Information). Using this inhibition model, a fitting equation (1) was constructed:

$$[F](t) = [M]_0(1 - exp(-k_f[E]t)) \quad (1)$$

where $[F]$ and $[M]_0$ are the concentration of the monomeric form and fibrillated form of αSyn, respectively, and $[E]$ is the equilibrium concentration of active fibril ends. We thus evaluated the changes in the parameter $[E]$ by fitting the aggregation curves.

The elongation profiles of 50 μM of αSyn in the absence and presence of various concentrations of BD1–GKKK (1–100 μM) were generated by the addition of 5 % seeds of preformed fibrils (Figure 5B). Since the rate of fibril elongation R is proportional to the concentration of active fibril ends ($R = k_f[E][M]$), the ratio of the reaction rate in the presence and the absence of BD1–GKKK (R/R_0) is equal to the fraction of active fibril ends ($R/R_0 = [E]/[E]_0 = K_D/(K_D + [\text{BD1–GKKK}])$), where K_D is the dissociation constant (see the Supporting Information). The kinetic data obtained using the above fitting model indicated that the growth of fibrils was decelerated in the presence of BD1–GKKK (Figure 5C). The magnitude of ThT intensity reached almost the same value at the end of the reaction below 0.5 molar equivalent of BD1–GKKK, implying that there could be no morphological change of aggregates that would affect the growth rate of fibrils. Above 0.5 molar equivalent of BD1–GKKK, the magnitude of ThT at the end of the reaction decreased (Figure 5B). We expected that the decrease of free monomer concentration of αSyn has occurred at high concentrations of BD1–GKKK presumably caused by the formation of small irreversible complexes of αSyn and BD1–GKKK which is out of the reaction model in Figure 5A. Indeed, with individual AFM images of the initial state of each solution, we confirmed small assemblies were formed in the presence of 2.0 molar equivalent of BD1–GKKK (Figure 5D). Histogram of height represents the distribution of oligomer-size assemblies (< 2 nm) in the presence of BD1–GKKK (Figure 5E).

Taken together, we propose two possible inhibitory mechanisms, a kinetic inhibition suppressing the rate of αSyn aggregation and a thermodynamic inhibition redirecting the αSyn fibril formation process to the formation of modified aggregates species. At a low range of concentrations of BD1–GKKK (0.02–0.5 molar equivalent), it can prolong the lag phase of αSyn aggregation (Figure 3C) and decelerate the elongation rate of αSyn fibrils in a concentration-dependent manner (Figure 5B, C). By contrast, at a higher range of

concentration, αSyn seems to form non-fibrillar aggregated species rapidly (Figure 5D, E), resulting in a reduction of the mass of fibrils. Based on the observation that BD1–GKKK binds to the surface of αSyn fibrils and inhibits fibril growth (Figure 4, 5), we conclude that the kinetically trapped off-pathway intermediate formed by the addition of BD1–GKKK is a state of αSyn fibril whose the growth terminus of fibrils is capped with BD1–GKKK, and thus interrupt subsequent monomer binding of αSyn. Therefore, apparent expansions of the lag phase in the spontaneous αSyn fibril formation appeared to be a result of the binding of BD1–GKKK to an early species in the αSyn aggregation process. In this inhibitory mechanism, the structurally constrained macrocycle may be an appropriate scaffold based on the fact that it can effectively block the propagation of fibril structure by creating steric hindrance. Since the number of active growth termini of fibrils should be lower than the number of monomeric species, the inhibition could occur at low stoichiometric concentrations. This low stoichiometric inhibition manner would favor the maintenance of protein homeostasis in the cell.

Cellular effects of BD1–GKKK on deposition of αSyn aggregates

We further evaluated the effects of BD1–GKKK on the formation of αSyn aggregates in the mouse Neuro-2a (N2a) cells. When αSyn with GFP fused to their C-terminal were stably expressed in cells (N2a–αSyn–GFP), and theαSyn fibril seeds aggregated the endogenous αSyn–GFP, resulting in the formation of visible green dot signals inside of cells (Figure 6A). Prior to such aggregation assays, we tested the cellular toxicity of BD1–GKKK in the N2a–αSyn–GFP cells by means of lactate dehydrogenase activity (LDH) assay and cell counting (Figure S6). Incubation of the cells with BD1–GKKK did not show cytotoxic activity in the range of 1–30 μM. In the absence of BD1–GKKK, αSyn–GFP in the cells was condensed by transfection of pre-formed fibrils (PFF), whereas cells treated with BD1–GKKK showed less condensation of αSyn–GFP (Figure 6B). Their fluorescent images clearly showed a significant decrease in the number and area of fluorescent dots in a BD1–GKKK concentration-dependent manner (Figure 6C), suggesting that the amount of αSyn assemblies was reduced. These results suggest that BD1–GKKK inhibits seed-dependent propagation process of αSyn aggregation in the cell system.

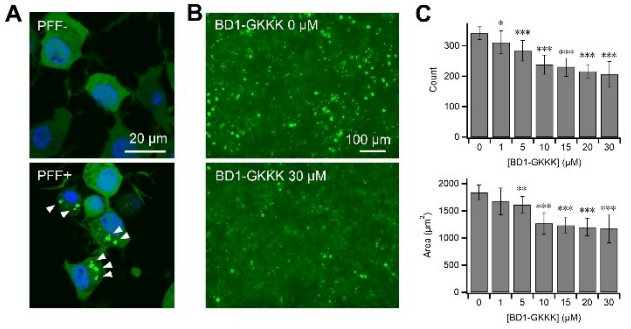

Figure 6. BD1–KKK inhibits the aggregation of αSyn–GFP in the N2a-αSyn–GFP cells. (*A*) Preformed fibrils (PFFs) treatment induced αSyn aggregation in the N2a-αSyn–GFP cells. Cell nuclei were stained with Hoechst (blue). (*B*, *C*) The effect of BD1–GKKK against the PFF-induced aggregation of αSyn–GFP in the cells. Representative fluorescence images of cells (*B*) and the number of αSyn–GFP aggregates and the total area of aggregates at various concentrations of BD1–GKKK (*C*) are shown. Cells are incubated for 48 h after treatment with the PFF and the peptides. The data represent the mean±STD for 12 replicates. The symbols *, **, and *** indicate $p < 0.05$, 0.01, 0.001, respectively.

Conclusion

In this report, we have shown that the RaPID system using thioether-macrocyclic peptide libraries has yielded a *de novo* peptide BD1 that acts as an inhibitor against the fibril formation of αSyn. Remarkably, it interferes with the αSyn aggregation process at low stoichiometries. Furthermore, a solubility-tag modified peptide, BD1–GKKK, enhanced the kinetic-based inhibition and showed complete inhibition in the observed time scale. A series of biophysical analyses have revealed the molecular mechanism of kinetic inhibition where BD1–GKKK binds with the fibril ends of αSyn and interrupts the growth of fibrils. This low stoichiometric inhibition of the aggregation of αSyn is consistent with our in vivo experiments using living cells overexpressing αSyn. Accordingly, the RaPID selection with macrocycle libraries will become a promising approach for discovering binders not only αSyn but also other disordered amyloidogenic proteins involved in diseases of the central nervous systems.

Acknowledgements

We thank Prof. Yuji Goto for discussing the results and commenting on the manuscript, and Dr. Komatsu and Dr. Naohiro Terasaka for TEM measurements. This work was supported by the Japan Society for the Promotion of Science (JSPS) Grant-in-Aid for Specially Promoted Research (JP20H05618) to H.S.; JSPS research fellow (JP18J00698) and Japan Science and Technology Agency (JST), ACT-X (JPMJAX2113) to T.I.; and JST to HY (JPMJMS2024-5) and RT (JPMJMS2024), EM measurement was supported by Nanotechnology Platform project by the Ministry of Education, Culture, Sport, Science, and Technology of Japan JPMXP09A21UT0030.

Conflict of Interests

The authors declare no conflict of interest.

Data Availability Statement

The data that support the findings of this study are available in the supplementary material of this article.

Keywords: alpha-synuclein · amyloid · inhibitor · Parkinson's disease · RaPID screening

[1] a) T. M. Dawson, V. L. Dawson, *Science* **2003**, *302*, 819–822; b) U. Dettmer, D. Selkoe, T. Bartels, *Curr. Opin. Neurobiol.* **2016**, *36*, 15–22; c) T. P. Knowles, M. Vendruscolo, C. M. Dobson, *Nat. Rev. Mol. Cell Biol.* **2014**, *15*, 384–396.

[2] a) V. M. Lee, J. Q. Trojanowski, *Neuron* **2006**, *52*, 33–38; b) M. Perni, C. Galvagnion, A. Maltsev, G. Meisl, M. B. Muller, P. K. Challa, J. B. Kirkegaard, P. Flagmeier, S. I. Cohen, R. Cascella, S. W. Chen, R. Limbocker, P. Sormanni, G. T. Heller, F. A. Aprile, N. Cremades, C. Cecchi, F. Chiti, E. A. Nollen, T. P. Knowles, M. Vendruscolo, A. Bax, M. Zasloff, C. M. Dobson, *Proc. Natl. Acad. Sci. USA* **2017**, *114*, E1009–E1017; c) B. M. Burmann, J. A. Gerez, I. Matecko-Burmann, S. Campioni, P. Kumari, D. Ghosh, A. Mazur, E. E. Aspholm, D. Sulskis, M. Wawrzyniuk, T. Bock, A. Schmidt, S. G. D. Rudiger, R. Riek, S. Hiller, *Nature* **2020**, *577*, 127–132.

[3] G. Toth, S. J. Gardai, W. Zago, C. W. Bertoncini, N. Cremades, S. L. Roy, M. A. Tambe, J. C. Rochet, C. Galvagnion, G. Skibinski, S. Finkbeiner, M. Bova, K. Regnstrom, S. S. Chiou, J. Johnston, K. Callaway, J. P. Anderson, M. F. Jobling, A. K. Buell, T. A. Yednock, T. P. Knowles, M. Vendruscolo, J. Christodoulou, C. M. Dobson, D. Schenk, L. McConlogue, *PLoS One* **2014**, *9*, e87133.

[4] a) J. T. Jarrett, P. T. Lansbury, Jr., *Cell* **1993**, *73*, 1055–1058; b) H. Kitayama, Y. Yoshimura, M. So, K. Sakurai, H. Yagi, Y. Goto, *Biochim. Biophys. Acta* **2013**, *1834*, 2640–2646; c) T. Ikenoue, Y. H. Lee, J. Kardos, H. Yagi, T. Ikegami, H. Naiki, Y. Goto, *Proc. Natl. Acad. Sci. USA* **2014**, *111*, 6654–6659; d) Y. Lin, Y. H. Lee, Y. Yoshimura, H. Yagi, Y. Goto, *Langmuir* **2014**, *30*, 1845–1854.

[5] a) N. Cremades, S. I. Cohen, E. Deas, A. Y. Abramov, A. Y. Chen, A. Orte, M. Sandal, R. W. Clarke, P. Dunne, F. A. Aprile, C. W. Bertoncini, N. W. Wood, T. P. Knowles, C. M. Dobson, D. Klenerman, *Cell* **2012**, *149*, 1048–1059; b) P. Alam, L. Bousset, R. Melki, D. E. Otzen, *J. Neurochem.* **2019**, *150*, 522–534.

[6] a) P. Arosio, T. C. Michaels, S. Linse, C. Mansson, C. Emanuelsson, J. Presto, J. Johansson, M. Vendruscolo, C. M. Dobson, T. P. Knowles, *Nat. Commun.* **2016**, *7*, 10948; b) J. Habchi, P. Arosio, M. Perni, A. R. Costa, M. Yagi-Utsumi, P. Joshi, S. Chia, S. I. A. Cohen, M. B. D. Muller, S. Linse, E. A. A. Nollen, C. M. Dobson, T. P. J. Knowles, M. Vendruscolo, *Sci. Adv.* **2016**, *2*; c) J. Habchi, S. Chia, R. Limbocker, B. Mannini, M. Ahn, M. Perni, O. Hansson, P. Arosio, J. R. Kumita, P. K. Challa, S. I. Cohen, S. Linse, C. M. Dobson, T. P. Knowles, M. Vendruscolo, *Proc. Natl. Acad. Sci. USA* **2017**, *114*, E200–E208; d) F. A. Aprile, P. Sormanni, M. Perni, P. Arosio, S. Linse, T. P. J. Knowles, C. M. Dobson, M. Vendruscolo, *Sci. Adv.* **2017**, *3*, e1700488; e) S. I. A. Cohen, P. Arosio, J. Presto, F. R. Kurudenkandy, H. Biverstal, L. Dolfe, C. Dunning, X. Yang, B. Frohm, M. Vendruscolo, J. Johansson, C. M. Dobson, A. Fisahn, T. P. J. Knowles, S. Linse, *Nat. Struct. Mol. Biol.* **2015**, *22*, 207–213; f) A. Munke, J. Persson, T. Weiffert, E. De Genst, G. Meisl, P. Arosio, A. Carnerup, C. M. Dobson, M. Vendruscolo, T. P. J. Knowles, S. Linse, *Proc. Natl. Acad. Sci. USA* **2017**, *114*, 6444–6449.

[7] a) V. Armiento, A. Spanopoulou, A. Kapurniotu, *Angew. Chem. Int. Ed.* **2020**, *59*, 3372–3384; b) T. Arai, T. Araya, D. Sasaki, A. Taniguchi, T. Sato, Y. Sohma, M. Kanai, *Angew. Chem. Int. Ed.* **2014**, *53*, 8236–8239; c) P. N. Cheng, C. Liu, M. Zhao, D. Eisenberg, J. S. Nowick, *Nat. Chem.* **2012**, *4*, 927–933.

[8] a) T. Ikenoue, F. A. Aprile, P. Sormanni, F. S. Ruggeri, M. Perni, G. T. Heller, C. P. Haas, C. Middel, R. Limbocker, B. Mannini, T. C. T. Michaels, T. P. J. Knowles, C. M. Dobson, M. Vendruscolo, *Sci. Rep.* **2020**, *10*, 15280; b) P. Sormanni, F. A. Aprile, M. Vendruscolo, *Proc. Natl. Acad. Sci. USA* **2015**, *112*, 9902–9907.

[9] a) G. T. Heller, P. Sormanni, M. Vendruscolo, *Trends Biochem. Sci.* **2015**, *40*, 491–496; b) G. T. Heller, M. Bonomi, M. Vendruscolo, *J. Mol. Biol.* **2018**, *430*, 2288–2292; c) G. T. Heller, F. A. Aprile, T. C. T. Michaels, R. Limbocker, M. Perni, F. S. Ruggeri, B. Mannini, T. Lohr, M. Bonomi, C. Camilloni, A. De Simone, I. C. Felli, R. Pierattelli, T. P. J. Knowles, C. M. Dobson, M. Vendruscolo, *Sci. Adv.* **2020**, *6*, eabb5924.

[10] a) M. D. Tuttle, G. Comellas, A. J. Nieuwkoop, D. J. Covell, D. A. Berthold, K. D. Kloepper, J. M. Courtney, J. K. Kim, A. M. Barclay, A. Kendall, W. Wan, G. Stubbs, C. D. Schwieters, V. M. Lee, J. M. George, C. M. Rienstra, *Nat. Struct. Mol. Biol.* **2016**, *23*, 409–415; b) B. Li, P. Ge, K. A. Murray, P. Sheth, M. Zhang, G. Nair, M. R. Sawaya, W. S. Shin, D. R. Boyer, S. Ye, D. S. Eisenberg, Z. H. Zhou, L. Jiang, *Nat. Commun.* **2018**, *9*, 3609.

[11] K. Ito, T. Passioura, H. Suga, *Molecules* **2013**, *18*, 3502–3528.

[12] Y. Goto, T. Katoh, H. Suga, *Nat. Protoc.* **2011**, *6*, 779–790.

[13] a) S. Chen, D. Bertoldo, A. Angelini, F. Pojer, C. Heinis, *Angew. Chem. Int. Ed.* **2014**, *53*, 1602–1606; b) A. Angelini, L. Cendron, S. Chen, J. Touati, G. Winter, G. Zanotti, C. Heinis, *ACS Chem. Biol.* **2012**, *7*, 817–821; c) N. Bionda, R. Fasan, *ChemBioChem* **2015**, *16*, 2011–2016.

[14] a) S. I. Cohen, S. Linse, L. M. Luheshi, E. Hellstrand, D. A. White, L. Rajah, D. E. Otzen, M. Vendruscolo, C. M. Dobson, T. P. Knowles, *Proc. Natl. Acad. Sci. USA* **2013**, *110*, 9758–9763; b) T. C. T. Michaels, A. Saric, J. Habchi, S. Chia, G. Meisl, M. Vendruscolo, C. M. Dobson, T. P. J. Knowles, *Annu. Rev. Phys. Chem.* **2018**, *69*, 273–298.

[15] a) M. Adachi, M. Noji, M. So, K. Sasahara, J. Kardos, H. Naiki, Y. Goto, *J. Biol. Chem.* **2018**, *293*, 14775–14785; b) T. Miti, M. Mulaj, J. D. Schmit, M. Muschol, *Biomacromolecules* **2015**, *16*, 326–335; c) Y. Yoshimura, Y. Lin, H. Yagi, Y. H. Lee, H. Kitayama, K. Sakurai, M. So, H. Ogi, H. Naiki, Y. Goto, *Proc. Natl. Acad. Sci. USA* **2012**, *109*, 14446–14451; d) M. Adachi, M. So, K. Sakurai, J. Kardos, Y. Goto, *J. Biol. Chem.* **2015**, *290*, 18134–18145.

[16] a) V. N. Uversky, *F1000Research* **2017**, *6*, 525; b) T. Bachhuber, N. Katzmarski, J. F. McCarter, D. Loreth, S. Tahirovic, F. Kamp, C. Abou-Ajram, B. Nuscher, A. Serrano-Pozo, A. Muller, M. Prinz, H. Steiner, B. T. Hyman, C. Haass, M. Meyer-Luehmann, *Nat. Med.* **2015**, *21*, 802–807; c) B. K. Choi, J. Y. Kim, M. Y. Cha, I. Mook-Jung, Y. K. Shin, N. K. Lee, *Biochemistry* **2015**, *54*, 1831–1840; d) U. Sengupta, M. J. Guerrero-Munoz, D. L. Castillo-Carranza, C. A. Lasagna-Reeves, J. E. Gerson, A. A. Paulucci-Holthauzen, S. Krishnamurthy, M. Farhed, G. R. Jackson, R. Kayed, *Biol. Psychiatry* **2015**, *78*, 672–683; e) G. M. Pocas, J. Branco-Santos, F. Herrera, T. F. Outeiro, P. M. Domingos, *Hum. Mol. Genet.* **2015**, *24*, 1898–1907.

[17] G. T. Heller, F. A. Aprile, M. Bonomi, C. Camilloni, A. De Simone, M. Vendruscolo, *J. Mol. Biol.* **2017**, *429*, 2772–2779.

[18] a) V. V. Shvadchak, K. Afitska, D. A. Yushchenko, *Angew. Chem. Int. Ed.* **2018**, *57*, 5690–5694; b) E. D. Agerschou, V. Borgmann, M. M. Wordehoff, W. Hoyer, *Chem. Sci.* **2020**, *11*, 11331–11337; c) Y. Ohhashi, Y. Hagihara, G. Kozhukh, M. Hoshino, K. Hasegawa, I. Yamaguchi, H. Naiki, Y. Goto, *J. Biochem.* **2002**, *131*, 45–52.

[19] a) H. H. Lee, T. S. Choi, S. J. Lee, J. W. Lee, J. Park, Y. H. Ko, W. J. Kim, K. Kim, H. I. Kim, *Angew. Chem. Int. Ed.* **2014**, *53*, 7461–7465; b) S. A. Sievers, J. Karanicolas, H. W. Chang, A. Zhao, L. Jiang, O. Zirafi, J. T. Stevens, J. Munch, D. Baker, D. Eisenberg, *Nature* **2011**, *475*, 96–100.

Manuscript received: April 21, 2023
Accepted manuscript online: April 25, 2023
Version of record online: ■■, ■■

RESEARCH ARTICLE

Although inhibition of α-synuclein aggregation is an appealing approach for the prevention of this neurodegenerative pathology, the development of a binder has been yet challenging because of the disordered nature of α-synuclein. Here, by means of the RaPID system, we discovered a macrocycle inhibitor for the formation of α-synuclein aggregation at low stoichiometries.

Dr. T. Ikenoue, Dr. M. Oono, Dr. M. So, Dr. H. Yamakado, Prof. T. Arata, Prof. R. Takahashi, Prof. Y. Kawata, Prof. H. Suga**

1 – 8

A RaPID Macrocyclic Peptide That Inhibits the Formation of α-Synuclein Amyloid Fibrils